XIX. GASEOUS ELECTRONICS*

Academic and Research Staff

Prof. G. Bekefi
Prof. W. P. Allis
Prof. S. C. Brown
Prof. B. L. Wright
J. J. McCarthy
W. J. Mulligan

Graduate Students

G. A. Garosi

RESEARCH OBJECTIVES

Our general objectives are concerned with the study of atomic and molecular processes and with the transport of charged particles in weakly ionized collision-dominated plasmas. During the past year our efforts in this field have been on a rather modest scale. The research that we have conducted was concerned with the effects of pipe turbulence on the electrical conductivity and on the diffusion processes in an Argon plasma. This work has come to a successful conclusion and we plan to terminate it soon.

In the future we plan to devote our efforts to those problems in gaseous electronics that are relevant to the physics of gas lasers. In particular, we intend to look into problems of striations, sound propagation, and mode locking.

G. Bekefi

A. PARTICLE LOSS IN A TURBULENT, WEAKLY IONIZED, ARGON DISCHARGE

This report presents further studies performed on the turbulent Argon plasma which were previously reported.[1-3] The main emphasis in this report is on the effects of the gas flow on the charged particle loss rate.

1. Afterglow Plasma

In a previous report[3] it was explained that an afterglow experiment was performed in order to measure directly the effect of turbulent gas flow on the plasma loss mechanism. The experimental arrangement is shown in Fig. XIX-1. The first probe (No. 1) at the right of the anode is located 0.5 cm from the center of this electrode and the last probe (No. 8) is located 9.5 cm from the first. All probes are positioned on the tube axis.

It was also mentioned previously that the sheath thickness can no longer be neglected for probes collecting ion saturation current in the decaying plasma. A direct calculation of the sheath thickness was not attempted because the appropriate expression[1,4] involves the ion saturation current density, a quantity which is unknown unless the sheath

*This work was supported by the Joint Services Electronics Programs (U. S. Army, U. S. Navy, and U. S. Air Force) under Contract DA 28-043-AMC-02536(E).

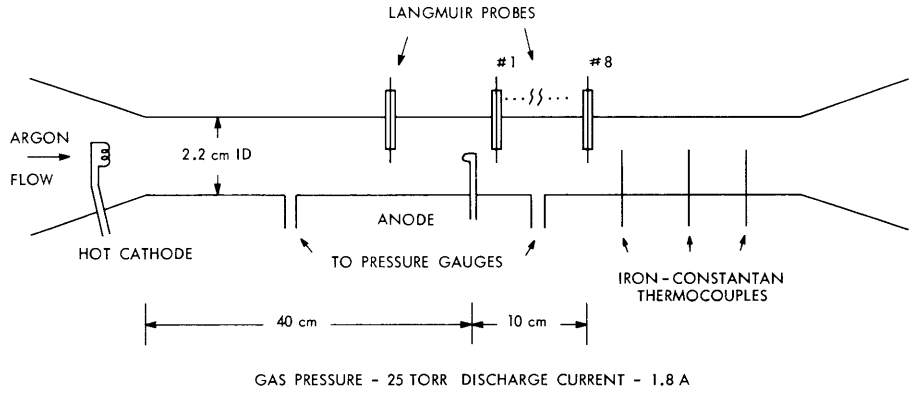

Fig. XIX-1. Tube for spatial afterglow experiment.

size is known. Such a calculation would require a time-consuming iterative process. The effects of the finite sheath size can be taken into account more readily by extending the ion saturation part of the probe's I-V characteristics up to the plasma potential where the sheath thickness is essentially zero; that is, we make use of the fact that the expression for the sheath thickness is a monotonically increasing function of $V = V_c - V_p$, where V_c is the bias on the probe, and V_p is the plasma potential, and that it goes to zero as V goes to zero. This method is illustrated symbolically in Fig. XIX-2. A calculation based on the expression for the sheath thickness shows that this graphic method introduces an

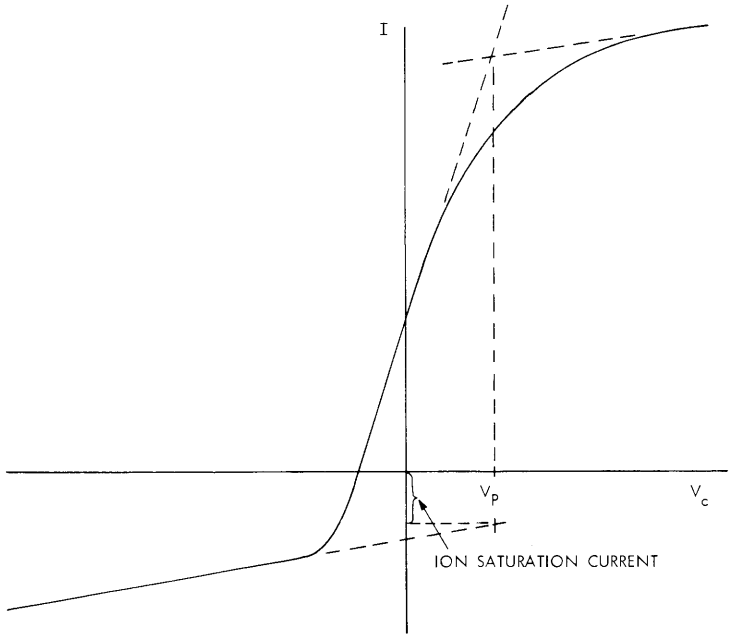

Fig. XIX-2. Method for determining ion saturation current.

error of up to 20% in the determination of the ion saturation current density. In Fig. XIX-3 some representative data taken in the afterglow are plotted. The ordinate $(I_+)_{so}$ is proportional to the electron density. The abscissa is the time in the frame of reference of the decaying, flowing plasma given by $d/\bar{U}$, where d is the distance from the downstream electrode to the probe, and $\bar{U}$ is the mean gas flow velocity.

The important things to note about the plots are, first, that the decay is exponential over more than one decade in density, thereby permitting us to obtain a unique time constant or loss rate, ν_L. Second, the increase of the slope, and thus of the loss rate with the increase in Reynolds number, Re.

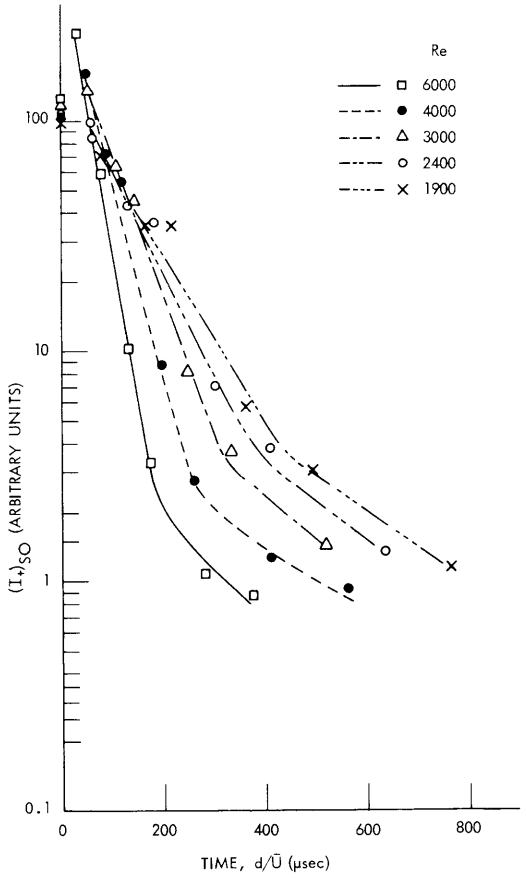

Fig. XIX-3. Afterglow data.

A plot of the loss rate, ν_L, against the flow parameter, Q_o, is given in Fig. XIX-4. The afterglow data are represented by open circles. The Reynolds number scale is also shown for reference. Note that the afterglow data do not extend below a Reynolds number of ~1500.

It is possible, of course, to obtain the loss rate in the active discharge by calculating

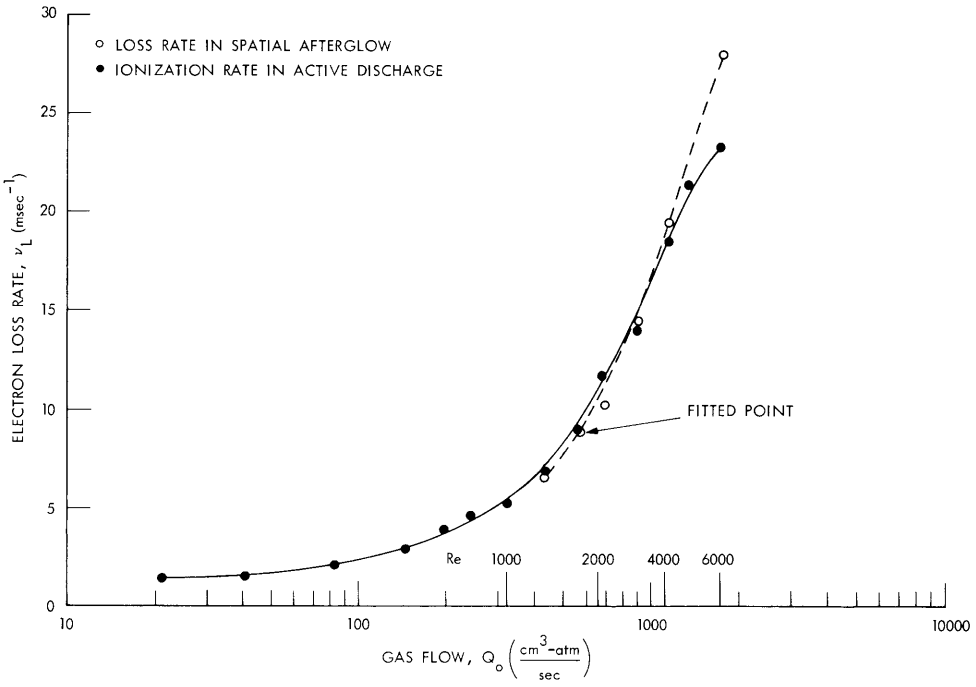

Fig. XIX-4. Experimentally determined electron loss rate.

the ionization frequency. The exponential decay of the electron density shown in Fig. XIX-3 suggests that the loss rate in the early afterglow is equal to the loss rate in the active discharge region. The computed values of the ionization frequency, ν_i, are also plotted in Fig. XIX-4. The ionization frequency curve was fitted to the measured loss rate at one value of flow. The method used to compute ν_i will now be discussed.

2. Ionization Frequency

The expression used to compute ν_i is based on work done by Karl Wojaczek[5] and is given by

$$\nu_i = C \frac{n}{V_e^{3/2}} \exp\left[-\frac{11.5}{V_e}\right], \tag{1}$$

where C is a known constant, V_e is the electron temperature in Volts, n is the electron density, and 11.5 is the excitation energy of the metastable level. The expression is based on a stepwise ionization process mainly from the metastable level, under the assumption that the metastables are lost mainly via ionization. A further assumption is $V_e \ll 11.5$ Volts. The expression has been slightly simplified, because of the conditions of the discharge.

The ionization frequency was calculated for the conditions in the center of the plasma column. As was shown previously,[3] the plasma density fluctuation can be interpreted as resulting from the thrashing about of the constricted positive column under the influence of the neutral-particle fluctuations. The electron density at the center of the plasma column, n_o, which is needed in the computation of ν_i, can be obtained from measurements by using a form of Eq. 6 from the previous report[3] as shown here

$$n_o = \frac{\langle \rho^2 \rangle + \langle R^2 \rangle}{\langle \rho^2 \rangle} \langle n(0) \rangle, \tag{2}$$

where $\langle n(0) \rangle$ is the electron density as measured in the center of the tube, and $\langle \rho^2 \rangle$ and $\langle R^2 \rangle$ are parameters used to specify the electron density profile and the intensity of the thrashing, respectively. (The factor $\langle \rho^2 \rangle$ in the denominator of Eq. 2 was inadvertently left out of both Eqs. 6 and 7 in the previous report.[3])

The electron temperature as measured from single probe I-V characteristics is shown as a function of gas flow in Fig. XIX-5. Because of the extreme sensitivity of ν_i to electron temperature and because of the inaccuracy inherent in this method of measuring V_e,[4] the measured values were compared with values predicted by the conservation equation for electron energy.

On account of the low degree of ionization (≈0.001%) and the high pressure (25 Torr) associated with this experiment, the electron energy can be accounted for, to a good approximation, by balancing the ohmic heating term against the electron-neutral elastic energy transfer term.[6, 7] These terms are approximately given by

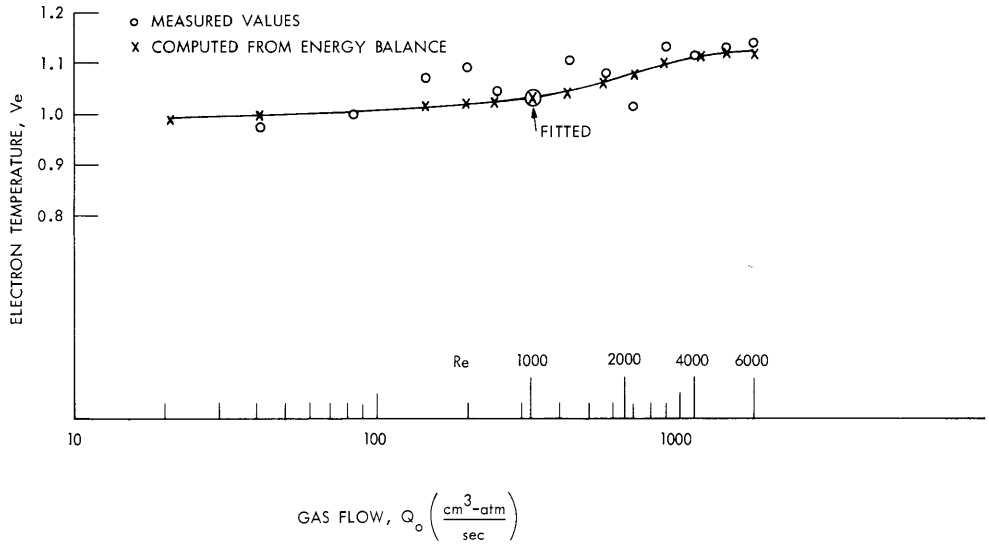

Fig. XIX-5. Electron temperature dependence on flow.

$$\frac{3}{2} k(T_e - T)\, \gamma_m \nu_{en} = e\mu_e E_o^2, \tag{3}$$

where T_e and T are the electron and gas temperatures, respectively, k is Boltzmann's constant, ν_{en} is the electron-neutral collision frequency, μ_e is the electron mobility, e is the electronic charge, and E_o is the electric field. Furthermore, γ_m is the fractional energy loss by the electrons per collision and is given for the case of elastic collisions by $\gamma_m = 2m/M$, where m and M represent the mass of the electron and of the atoms, respectively. The expressions used for ν_{en} and μ_e are those given by Rogoff.[8] Equation 3 can be written, for $T_e \gg T$, as

$$V_e = \left[.060\, E_o \frac{T}{p} \right]^{3/5}, \tag{4}$$

where p is the gas pressure.

The values of V_e calculated by means of Eq. 4 from measured values of E_o, T, and p are also shown in Fig. XIX-5. Fitting the calculated values to the measurements corresponds to replacing the factor 0.060 in Eq. 4 by 0.042. The agreement shown in Fig. XIX-5 indicates that the measured values of V_e are reliable.

The good agreement between ν_i and ν_L shown in Fig. XIX-4 is used to justify the assumptions made in the interpretation of the data in the active discharge and in the decaying plasma.

The rest of this report deals with a theoretical model proposed to explain the data represented in Fig. XIX-4.

3. Theoretical Model

The effect of fluctuations in the neutral gas on the plasma is given by the continuity equation

$$\frac{\partial n_j}{\partial t} + \nabla \cdot n_j v_j = n_j \nu_i - \alpha n_j^2; \quad j = i, e, \tag{5}$$

where n_j is the particle density, v_j is the particle velocity, α is the recombination coefficient, and i and e stand for ions and electrons, respectively. Expressing the density and velocity as

$$n_j = \bar{n}_j + n_j'; \quad v_j = \bar{v}_j + v_j'; \quad \bar{v}_j' = \bar{n}_j' = 0 \tag{6}$$

and applying Eq. 5 to the steady state we get

$$\nabla \cdot \left\{ (\bar{n}_j + n_j')(\bar{v}_j + v_j') \right\} = (\bar{n}_j + n_j')\nu_i - \alpha(\bar{n}_j + n_j')^2, \tag{7}$$

where fluctuations in the ionization frequency have been neglected.

If we now confine our attention to the central region of the plasma column, it is possible to neglect the volume recombination term. Time-averaging Eq. 7, we get

$$\nabla \cdot (\bar{n}_j \bar{v}_j + \overline{n'_j v'_j}) = \bar{n}_j \nu_i. \tag{8}$$

The time-averaging process has been done in the frame of reference of the thrashing plasma column. We shall return to this point.

We now make the usual assumptions that are valid in the regime of ambipolar diffusion, and, also, we ignore the component of $\bar{n}_j \bar{v}_j$ attributable to the discharge current, since this particle flux is assumed to be divergenceless. Equation 8 thus becomes

$$\{\nabla \cdot [-D_a \nabla \bar{n} + \overline{n'v'}]\}_r = \bar{n}\nu_i, \tag{9}$$

where D_a is the ambipolar diffusion coefficient, and we are to take the radial component of the divergence. It is also assumed that fluctuations in the charged-particle velocities are equal to the fluctuations in the neutral-particle velocity; that is, $v'_e = v'_i = v'_n = u'$.

For low flow values, $u' = 0$ and the loss is given by classical ambipolar diffusion. For higher flows the effect of small-scale eddies, that is, eddies smaller than the radius of the plasma column, on the transport of plasma can be represented by means of a turbulence diffusion coefficient, D_T; thus, we have

$$\overline{n'u'} = -D_T \nabla \bar{n}. \tag{10}$$

For statistically steady, homogeneous turbulence an expression for the turbulence diffusion coefficient has been given by Hinze[10]

$$D_T = \left[\overline{(u'_r)^2}\right]^{1/2} L, \tag{11}$$

where L is the scale of eddy diffusion and is essentially the scale length for coherent motion of a fluid element in the radial direction. By introducing the mean flow velocity, $\bar{U}$, Eq. 11 can be written

$$D_T = \left[\frac{\overline{(u'_r)^2}}{\bar{U}^2}\right]^{1/2} L\bar{U}. \tag{12}$$

For the case of fully developed turbulent pipe flow Laufer[11] has measured the following approximate values

$$\left[\frac{\overline{(u'_r)^2}}{\bar{U}^2}\right]^{1/2} \approx .03; \quad L \approx 0.3a,$$

where a is the radius of the tube. By fully developed turbulence we mean that the statistical properties of the turbulence are independent of the Reynolds number. Using Eqs. 10 and 12, we can write Eq. 9 as

$$\nu_i = \left\{ D_a + \left[\frac{\overline{(u_r')^2}}{\bar{U}^2} \right]^{1/2} L\bar{U} \right\} \frac{1}{\Lambda_o^2}, \tag{13}$$

where we have used $\nabla^2 n = -n/\Lambda^2$, and the subscript zero means that Λ is to be evaluated in the center of the plasma column.

As we have mentioned, the loss rate represented by Eq. 13 is computed in the frame of reference of the thrashing plasma column. We believe, however, that the motion of the column will cause the diffusion length, Λ, to be a function of time, because of the dependence of Λ on the position of the column relative to the center of the tube. This dependence of Λ on position arises because a significant displacement of the plasma column from the tube axis will cause a shortening of the column radius, and thus an increase in the plasma density gradient, on the side nearer the tube wall. It appears, then, that Λ decreases as the separation, R, of the plasma column axis from the tube axis increases. It is necessary to average Eq. 13 over all possible positions of the plasma column, and Eq. 13 becomes

$$\nu_i = [D_a + D_T] \left\langle \frac{1}{\Lambda_o^2} \right\rangle, \tag{14}$$

where both D_a and D_T are assumed to be independent of the averaging process.

The angular brackets in Eq. 14 thus represent an average over the thrashing motion of the plasma and, in some sense, can be considered as an ensemble average over the macroscopic motions of the plasma. The time average, on the other hand, can, in the same spirit, be considered as an average over the microscopic motions of the plasma.

In order to calculate values for $\left\langle 1/\Lambda_o^2 \right\rangle$, we shall use a one-dimensional model suggested by Schulz.[12] The effect of the thrashing on the diffusion length can be obtained by calculating its effect on the effective radius of the plasma. The diagram in Fig. XIX-6 represents the behavior, in time, of the thrashing plasma column. The abscissa, X, represents the radial coordinate in the case of cylindrical geometry and the positions $\pm a$ represent the boundaries of the vacuum vessel. The assumption is that a fluid element initially at position X_o will evolve in time along the path $X_1(t)$ given by

$$X_1(t) = X_o + \delta(t) \cos\left(\frac{\pi X_o}{2a}\right), \tag{15}$$

where $\delta(t)$ represents the thrashing of the column. The cosine term represents the fact

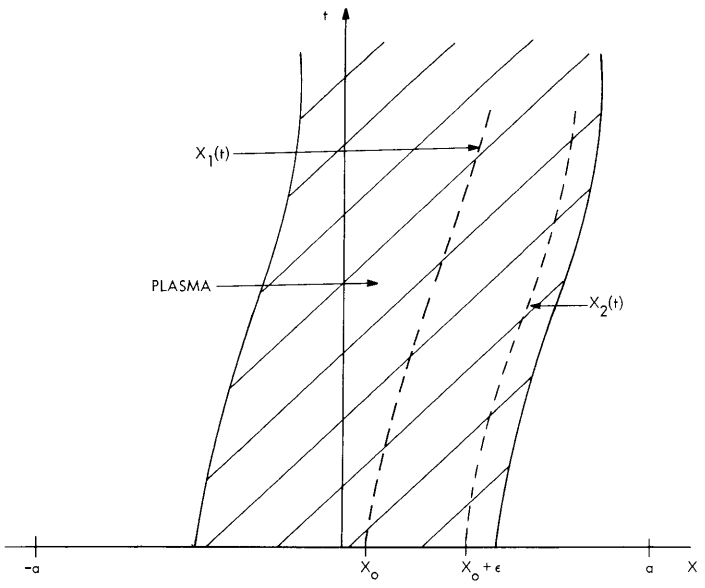

Fig. XIX-6. Time development of thrashing plasma.

that the parts of the column closer to the tube wall will not be displaced as far as the parts near the center of the column. A fluid element initially at position $X_o + \epsilon$ will evolve along the path

$$X_2(t) = X_o + \epsilon + \delta(t) \cos\left[\frac{\pi}{2a}(X_a+\epsilon)\right]. \tag{16}$$

If we now let X_o correspond to $X = 0$ when $\delta(t) = 0$, that is, the center of the plasma column, and let ϵ correspond to the "edge" of the plasma, then the half-width or "radius" of the plasma is given by

$$X_2(t) - X_1(t) = \epsilon + \delta(t)\left[\cos\left(\frac{\pi\epsilon}{2a}\right) - 1\right]. \tag{17}$$

By expanding the cosine term, the inverse of Eq. 17 becomes,

$$\frac{1}{X_2(t) - X_1(t)} = \frac{1}{\epsilon}\frac{1}{\left[1 - \frac{\epsilon}{2}\delta(t)\left(\frac{\pi}{2a}\right)^2\right]} \tag{18}$$

and

$$\frac{1}{(X_2(t)-X_1(t))^2} = \frac{1}{\epsilon^2}\sum_{m=0}^{\infty}(m+1)\left(\frac{\epsilon}{2}\right)^m\left[\delta(t)\left(\frac{\pi}{2a}\right)^2\right]^m. \tag{19}$$

To evaluate Eq. 19, we assume that there is a dominant frequency associated with the thrashing of the plasma. Then

$$\delta(t) = \delta_o \cos \omega t. \tag{20}$$

The amplitude, δ_o, is found by associating $\delta(t)$ with the intensity of the thrashing as obtained previously.[3] The association made is that

$$\langle \delta^2 \rangle = \frac{\delta_o^2}{2} = \langle R^2 \rangle, \tag{21}$$

where, as stated before, R is the displacement of the center of the plasma column from the tube axis. Averaging Eq. 19, we obtain

$$\left\langle \frac{1}{(X_2 - X_1)^2} \right\rangle = \frac{1}{\epsilon^2} \sum_{n=0}^{\infty} \frac{(2n+1)!!}{2n!!} \left(\frac{\pi}{2\sqrt{2}\, a} \right)^{4n} \epsilon^{2n} [2 \langle R^2 \rangle]^n. \tag{22}$$

We now identify ϵ with the width of the plasma column, $\langle \rho^2 \rangle$, as introduced and computed previously.[3] To obtain the diffusion length, we assume that the geometric factor relating the diffusion length to the "radius," $x_2 - x_1$, is a constant independent of the averaging process. Thus

$$\left\langle \frac{1}{\Lambda_o^2} \right\rangle = \frac{C}{\langle \rho^2 \rangle} \underbrace{\left[\sum_{n=0}^{\infty} \frac{(2n+1)!!}{2n!!} \left(\frac{\pi}{2}\right)^{4n} \left(\frac{1}{2}\right)^n \left(\frac{\langle \rho^2 \rangle}{a^2} \right)^n \left(\frac{\langle R^2 \rangle}{a^2} \right)^n \right]}_{A}, \tag{23}$$

where C is the geometric factor relating Λ_o^{-2} to $\langle \rho^2 \rangle^{-1}$ and must be considered here as an adjustable parameter. Combining Eqs. 12, 14, and 23, we get

$$\nu_L = \nu_i = [D_a + .01 \bar{U}]\, A\, \frac{C}{\langle \rho^2 \rangle} \tag{24}$$

In Fig. XIX-7 there is a comparison between the theoretical and the experimental loss rates. The plateau in the theoretical curve comes from the fact that the expression for the turbulence diffusion coefficient $D_T = 0.01\ U$ (Eq. 23) has been used in a region of flow and Reynolds number where it is not applicable. The assumption that the turbulence scale length, L, and the fractional rms velocity, $\sqrt{\overline{(u')^2}}/\bar{U}$, are constants for Re as low as 2500 is unrealistic. In computing ν_L from Eq. 24, D_T is assumed to be zero for $Q_o < 430$ cm^3-atm/sec.

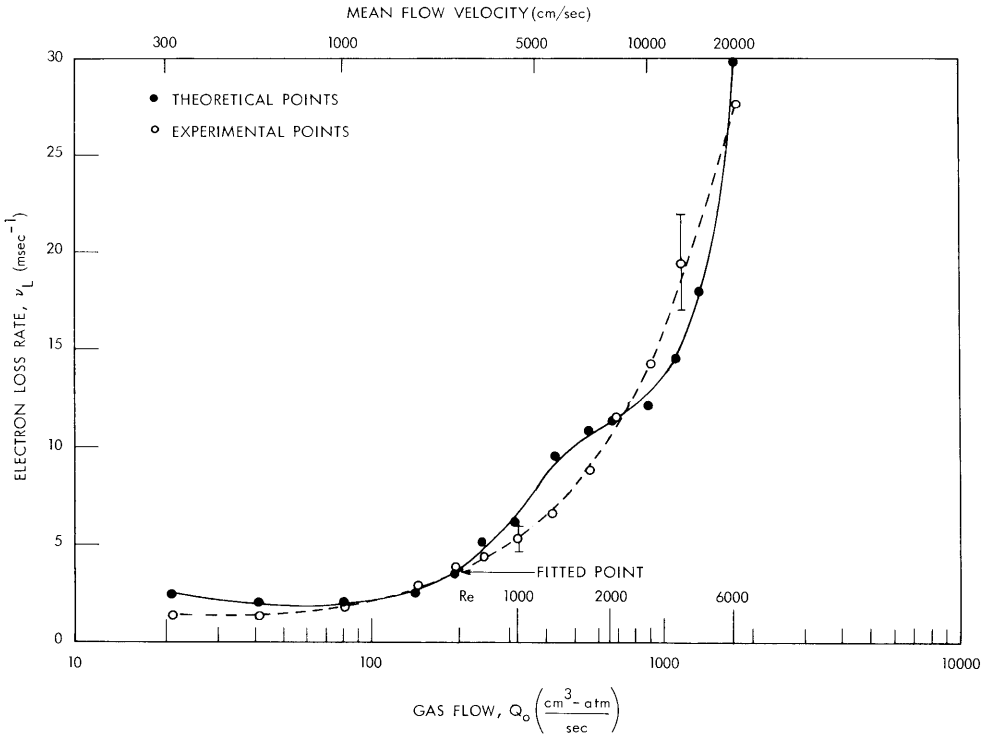

Fig. XIX-7. Comparison of theory and experiment for electron loss rate ν_L.

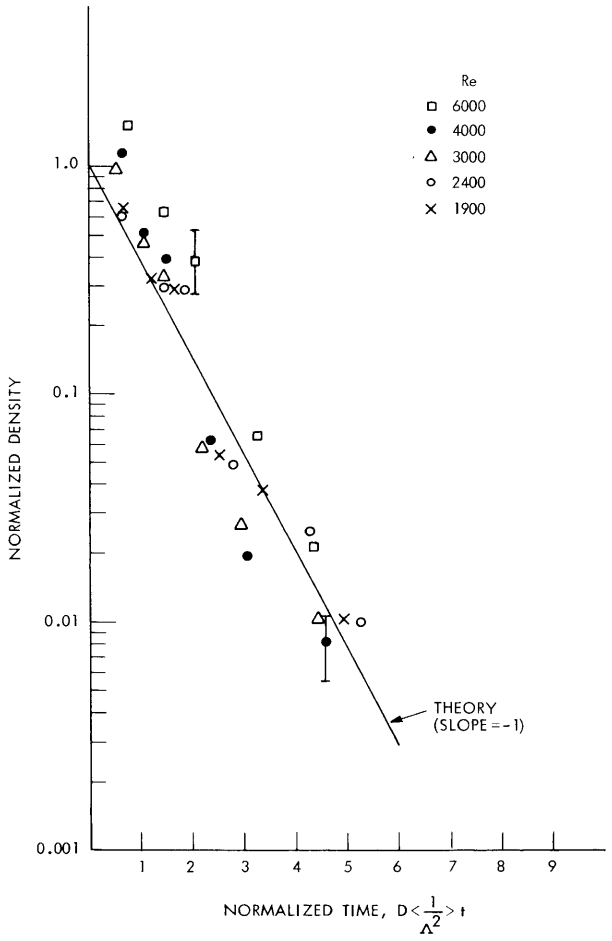

Fig. XIX-8. Comparison of density decay with theory.

For a decaying plasma, under the same assumptions as were applied to the active discharge, Eq. 5 becomes

$$\frac{\partial \bar{n}}{\partial t} = -[D_a + D_T] \left\langle \frac{1}{\Lambda_o^2} \right\rangle \bar{n}, \tag{25}$$

and integrating, we get

$$\bar{n} = \bar{n}_o \exp\left[-D\left\langle \frac{1}{\Lambda_o^2} \right\rangle t\right], \tag{26}$$

where $D = D_a + D_T$. A plot of $\log_e (\bar{n}/\bar{n}_o)$ against $D \left\langle 1/\Lambda_o^2 \right\rangle t$ should yield a straight line with a slope of -1. In Fig. XIX-8 such a plot is shown for the measured density decay in the spatial afterglow.

Future work will include verification of the proposed models and analysis of the electrical conductivity.

G. A. Garosi

References

1. G. Garosi, Quarterly Progress Report No. 86, Research Laboratory of Electronics, M. I. T., July 15, 1967, pp. 129-134.
2. G. Garosi, Quarterly Progress Report No. 89, op. cit., April 15, 1968, pp. 99-109.
3. G. Garosi, Quarterly Progress Report No. 91, op. cit., October 15, 1968, pp. 105-114.
4. V. M. Zakharova et al., Soviet Physics – Tech. Phys. 5, 411 (1960).
5. K. Wojaczek, Beiträge aus dem Plasma Physik 5, 307 (1965); 6, 211 (1966).
6. G. Garosi, Doctoral thesis research, M. I. T., 1968.
7. B. Yu. Baranov and K. N. Ul'yanov, JETP – Letters 6, 121 (1967).
8. G. Rogoff, Quarterly Progress Report No. 90, Research Laboratory of Electronics, M. I. T., July 15, 1968, pp. 69-75.
9. W. P. Allis, Technical Report 299, Research Laboratory of Electronics, M. I. T., Cambridge, Mass., June 13, 1956, p. 22f.
10. J. O. Hinze, Turbulence (McGraw-Hill Book Company, Inc., New York, 1959), p. 42f.
11. J. Laufer, NACA Technical Report 1174, 1954; NACA Technical Note 2123, 1950.
12. M. Schulz, Private communications, 1968.